This is the accepted manuscript made available via CHORUS. The article has been published as:

Model-independent versus model-dependent interpretation of the SDSS-III BOSS power spectrum: Bridging the divide

Samuel Brieden, Héctor Gil-Marín, and Licia Verde

Phys. Rev. D **104**, L121301 — Published 7 December 2021

DOI: 10.1103/PhysRevD.104.L121301

Model-independent vs. model-dependent interpretation of the SDSS-III BOSS power spectrum: bridging the divide

Samuel Brieden,* Héctor Gil-Marín,† and Licia Verde‡
ICC, University of Barcelona, IEEC-UB, Martí i Franquès, 1, E-08028 Barcelona, Spain
(Dated: November 2, 2021)

The traditional clustering analyses of galaxy redshift surveys compress the clustering data into a set of late-time physical variables in a model-independent way. This approach has recently been extended by an additional *shape variable* encoding early-time physics information. We apply this new technique, *ShapeFit*, to SDSS-III BOSS data and show that it matches the constraining power of alternative, model-dependent approaches, which directly constrain the model's parameters adopting a cosmological model *ab-initio*. *ShapeFit* is ~ 30 times faster, model-independent, naturally splits early- and late-time variables, and enables a better control of observational systematics.

I. LARGE SCALE STRUCTURE CLUSTERING: INTERPRETATION

The traditional clustering analysis of large-scale structure (LSS) galaxy redshift surveys is done by compressing the power spectrum data products into physical variables in a largely model-independent way. These are the well known Alcock-Paczynski (AP) scaling factors $\alpha_\perp$, $\alpha_\parallel$ [1] and the amplitude of velocity fluctuations, $f\sigma_8$ [2, 3]. The AP scaling factors are obtained by observing the standard ruler provided by the Baryon Acoustic Oscillation (BAO) feature. The amplitude of velocity fluctuations is obtained from the modulation of clustering amplitude in redshift space as function of the angle from the line-of-sight. This provides a powerful compression: from power spectrum multipoles as function of scale and redshift, to three quantities, the physical variables, per redshift bin. These are the physical variables that are then compared to theory predictions, within a given cosmological model, to constrain the numerical values of the model's parameters. The value of this classic approach lies in the fact that the model dependence is introduced only at the very end of the process, leaving most of the analysis as model-independent as possible. In addition, this approach nicely disentangles information of the late-time universe from that of the early-time universe, which is particularly valuable for going beyond simple parameter-fitting and pursuing ways to test the model and its underlying assumptions. It has a drawback, however: the compression is not lossless. Its target is robustness, but this comes at a cost.

This approach is conceptually different from the way in which, for example, Cosmic Microwave Background (CMB) data are routinely analyzed. The CMB maps are compressed into angular power spectra (as done for galaxy clustering), but then these are directly used to constrain the values of the parameters of an adopted cosmological model. The so called "physical parameters" for the CMB were actually proposed in [4]. The original goal was to accelerate cosmological inference from CMB data, and some of these parameters are still employed to date for the computational speed-up they yield. But, in reality, the physical parameters capture phenomenological signatures of physical processes, and can then be interpreted *a posteriori* in terms of constraints on cosmological model parameters. The use of physical parameters in CMB analysis to produce model-independent constraints [5, 6] and further compress CMB observations is not mainstream, at least in part, for two reasons. The CMB gives us a snapshot of the photon-baryon plasma at recombination, so is located at a single cosmic epoch; moreover, CMB photons must cross the entire Universe from the last scattering surface to $z = 0$, making it difficult to disentangle early-times physics signatures from late-times ones (but see [7, 8]).

The galaxy power spectrum can also be interpreted in a way completely analogous to the way the CMB is analyzed. The development of relatively fast (significantly faster than N-body simulations) modelling techniques for the non-linear galaxy power spectrum (e.g., Effective Field Theory, EFT) has made this "full modeling" (FM) possible over the past couple of years ([9, 10] and references therein). It became quickly apparent that this newer approach produces much tighter constraints on cosmological parameters than the classic (compressed-variables based) approach, if galaxy clustering is analyzed without external datasets, or strong external priors. On the other hand, in a joint CMB+LSS analysis (e.g., [11]) the two perform very similarly.

However, there is significant value in analyzing and interpreting galaxy clustering alone, especially not in combination with early-time probes. Separate analyses of observations of disparate epochs of the Universe are key to shed light on recent cosmological tensions (e.g., [12]), and propose explanations in terms of deviations from the standard cosmological model (e.g., [13]).

Until very recently, the extra signal responsible for the spectacular improvement provided by the FM approach was not well understood. However [14] showed that

* sbrieden@icc.ub.edu; Also at Dept. de Física Quàntica i Astrofísica, Universitat de Barcelona, Martí i Franquès 1, E-08028 Barcelona, Spain.
† hectorgil@icc.ub.edu
‡ liciaverde@icc.ub.edu; Also at ICREA, Pg. Lluís Companys 23, Barcelona, E-08010, Spain

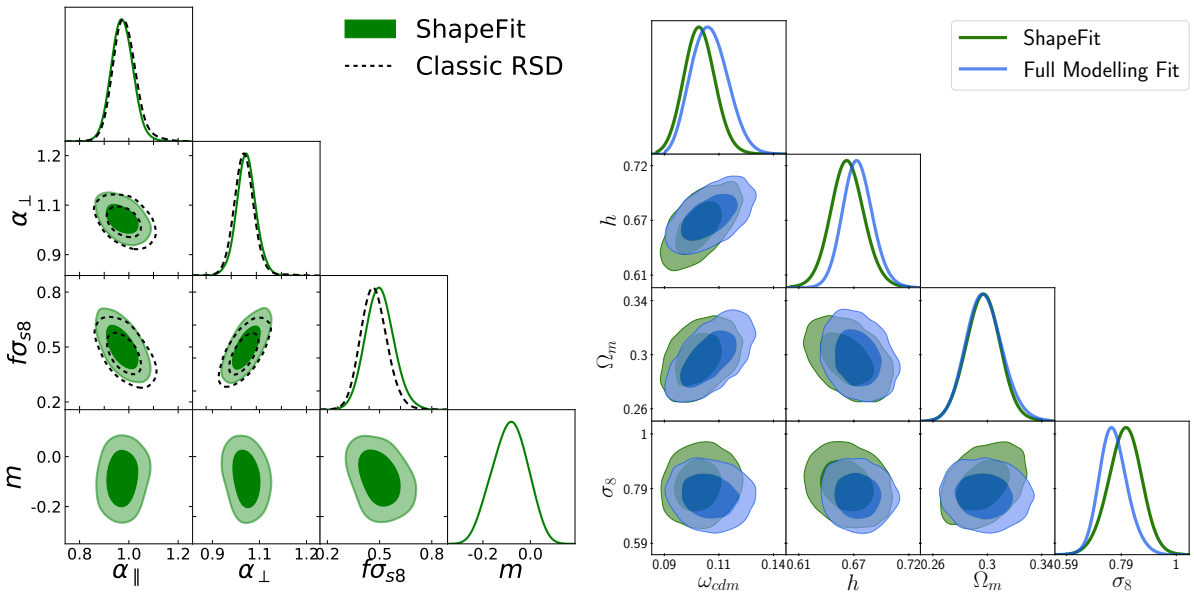


FIG. 1. *Left Panel*: compressed physical parameters posteriors derived from power spectra measurements of the BOSS high-redshift sample, $z_{\rm eff} = 0.61$ (constraints from the low-redshift sample, show a very similar behaviour). Black dashed contours display the classic RSD results, while novel *ShapeFit* results are shown in green. In both cases the 1-loop SPT theory has been used to model the monopole and quadrupole signals for $0.01 \leq k\,[h{\rm Mpc}^{-1}] \leq 0.15$. *Right Panel*: posteriors derived from low- and high-redshift samples of BOSS using the same scale-cuts as in the left panel. The blue contours correspond to the FM approach when a flat-ΛCDM model (+BBN Gaussian prior on ω_b) is directly fitted to the 224 power spectra multipoles bins, $P^{(\ell)}(k,z)$, using EFT to model the power spectrum. Conversely, green contours are drawn from the 8 compressed physical variables of *ShapeFit*, interpreted under the same cosmological model as for the blue contours.

a simple, one (phenomenological) parameter extension of the classic approach, *ShapeFit*, can capture most of this extra signal and provides the same statistical power within a flat-ΛCDM model. The compression that *ShapeFit* provides is nearly lossless for models that are effectively described, or well approximated, by wCDM-like models or simple variations of the CDM model at horizon scales at early times. While the classic approach (and *ShapeFit*) rely on a template for compression, it has been extensively demonstrated that the choice of the cosmological model necessary to create the template is unimportant, does not constitute a model prior and does not produce any significant systematic shifts under the correct interpretation of their physical variables [14–16].

In the classic RSD fit, at a given redshift bin z, the full power spectrum multipoles, $P^{(\ell)}(k,z)$, are compressed in just three physical variables sensitive to late-time physics only. These are two background-level variables that describe the cosmic expansion in units of the standard ruler, $\alpha_\parallel(z)$ and $\alpha_\perp(z)$ (see section 2.4 of [14]); and a perturbation-level variable that describes structures growth, $f\sigma_8(z)$. The extra information that the classic RSD neglects (and that the FM captures) is related to the shape of the transfer function. In addition to a more appropriate definition of velocity fluctuations $f\sigma_{s8}$, *ShapeFit* introduces a new variable m (see eqs. 3.5, 3.6 and 3.12 of [14] for definitions) which captures very well the bulk of the missing information. The physical interpretation of this m-variable is not any late-time physics phenomenon, but a series of early-time processes which modulate the broadband shape of the power spectrum (and the matter transfer function).

Hence, *ShapeFit* can be used to bridge the classic and FM approaches. The connection lies on making explicit and enforcing (or removing) a key "internal model prior which ties together early- and late-time compressed variables (see [14]). While the compressed physical variables are model-independent, the internal model prior connects the signature of early-time physics on the clustering signal on large scales, to the standard ruler signature constraining the late-time geometry and the redshift space signature of kinematics on the clustering.

II. APPLICATION TO SDSS-III BOSS DATA

We employ the Luminous Red Galaxy (LRG) samples of the SDSS-III BOSS survey [11], covering two non-overlapping redshift ranges: $0.2 < z < 0.5$ (effective redshift 0.38), containing 604,001 galaxies; and $0.5 < z < 0.75$ (effective redshift 0.61) containing 594,003 galaxies. As done in BOSS official papers, we treat these two redshift samples as uncorrelated. The effective volume traced by these two samples is $3.7\,{\rm Gpc}^3$ and $4.1\,{\rm Gpc}^3$, respectively, for a total effective volume of $7.8\,{\rm Gpc}^3$.

This same data set yields very different cosmological

constraints when it is analyzed using the classic approach or the FM fit (see e.g., fig 2 of [14] grey contours for classic RSD alone, orange when BAO post-reconstruction information is added, blue for FM fit). Both approaches yield very similar constraints when combined with a CMB prior (e.g., Planck; see the right panel of fig. 2 in [14]), as this type of prior effectively fixes the early-time physics information enclosed in the broadband shape.

In what follows, parameter constraints are obtained with a standard Markov Chain Monte Carlo (MCMC) posterior sampling [17]. The modeling of the clustering signal follows [9, 14] and employ the Boltzmann solver [18] including the EFT extension from [19]. The left panel of Fig. 1 displays the constraints on the late-time universe physical variables $\{\alpha_\parallel, \alpha_\perp, f\sigma_8\}$ obtained by the classic RSD analysis (dashed black contours) and by *ShapeFit* analysis, with the extra early-time universe parameter m (green contours), when both are applied to the high-redshift bin of BOSS.

The constraints on the three late-time universe physical parameters are not significantly modified by the addition of m as free extra variable, as m is essentially uncorrelated with them. The small correlation between m and, e.g., $f\sigma_8$ of -0.3 leads to only 5% increase in errors.

The posteriors of the left panel of Fig. 1 have been obtained without any strong model assumption [20], and hence are easily interpretable within a wide set of cosmological models. This model-interpretation process essentially places 'internal model priors' among the physical variables, connecting them with the internal parameters of the assumed model. This is shown by the green contours of the right panel of Fig. 1. The *ShapeFit* contours of the left panel (and additionally another set of four parameters at the low-redshift bin, $z_{\rm eff} = 0.38$) are interpreted within a flat-ΛCDM model with a Gaussian big bang nucleosynthesis (BBN) prior $\omega_b = 0.02268 \pm 0.00038$ [9, 21–23]; the resulting posteriors for $\{\omega_{cdm}, \Omega_m, h, \sigma_8\}$ are drawn. The constraints obtained by directly fitting the $P^{(\ell)}(k, z)$ shape on the same range of scales under the FM approach using EFT theory to describe the $P(k)$ modelling are shown in blue. Note the spectacular agreement between both approaches, especially considering that the green contours are obtained from just 8 variables (the 4 physical variables, $\{\alpha_\parallel, \alpha_\perp, f\sigma_8, m\}$ at two redshift bins), while blue contours are for 224 $P^{(\ell)}(k, z)$ measurements (28 k-bins measurements for two multipoles, two redshift bins, and two galactic hemispheres). Another advantage of *ShapeFit* over the FM approach is computational time. Once the compressed variables are extracted (since this step is model independent it only has to be done only once) the model-fitting is very fast: one model evaluation on a single-core is 8 times faster than the FM run. As the cosmological interpretation of *ShapeFit* parameters is done without any nuisance parameters and due to the much simpler likelihood surface, an MCMC needs 5-10 times fewer sampled points than the FM method for the same level of convergence. *ShapeFit* yields an overall speed-up factor of 40-80.

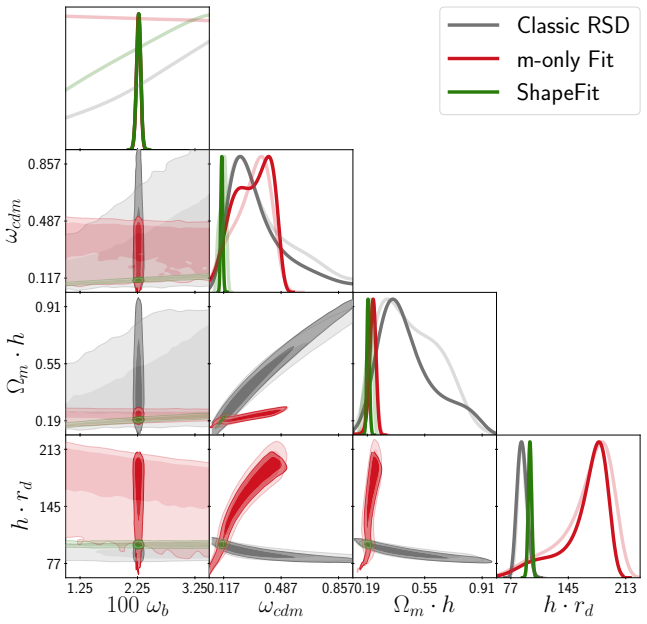


FIG. 2. Interpretation within a flat-ΛCDM model with a Gaussian BBN prior on $\omega_{\rm b}$ (opaque contours) and without (transparent contours), of different physical variables constraints from the low- and high-redshift BOSS samples. Gray correspond to classic RSD analysis based on late-time variables, $\{\alpha_\parallel(z), \alpha_\perp(z), f\sigma_8(z)\}$, red corresponds to the early-time shape variable $m(z)$ only, and their combination based on the ΛCDM internal model prior is shown in green.

III. THE POWER OF THE SHAPE VARIABLE

Fig. 2 shows the cosmological constraints for a standard flat-ΛCDM model, obtained from the low- and high-redshift BOSS samples using different sets of physical compressed variables. Gray contours arise from the classic RSD analysis using $\{\alpha_\parallel(z), \alpha_\perp(z), f\sigma_8(z)\}$, red contours from the *ShapeFit* analysis, but only using $m(z)$; green contours represent the *ShapeFit* analysis using the full combination of 4 physical variables per redshift-bin (as for the right panel of Fig. 1). The transparent contours are for a broad uniform prior, $0.005 < \omega_b < 0.04$, the opaque contours for the Gaussian BBN prior. Note, that relaxing the prior does not significantly affect the 1D posteriors measured by the classic RSD and m-only fit, but broadens the *ShapeFit* result on $\Omega_{\rm m}h$ by a factor ~ 2.5.

The choice of parameters shown, $\{\Omega_m h, hr_s, \omega_{cdm}, \omega_b\}$, highlights the complementary between the late- and the early-time physical variables. The BAO signal naturally constrains hr_s[24], while m constrains $\Omega_m h$, as this variable is directly governing the shape of the matter transfer function via matter-radiation equality epoch. The relation between m and $\Omega_m h$ is well approximated by the following fitting

formula valid in the range $0.1 < \Omega_m h < 0.35$

$$\frac{\Omega_m h}{\Omega_m^{\rm ref} h^{\rm ref}} = 0.13m^4 + 0.53m^3 + 0.86m^2 + m + 1 \ . \quad (1)$$

Within a ΛCDM model, the purely late-time (uncalibrated) expansion history constrains the ratio $\alpha_\parallel/\alpha_\perp$ (also the relative isotropic signals among z-bins). This can be used to measure Ω_m, which is particularly well constrained when low- and high-z samples are combined (see fig. 5 of [15]). In combination with the $\Omega_m h$ constraint provided by m, it is thus possible to produce a measurement of H_0. Note that, in spite of coming from galaxy clustering measurements, such measurement of H_0 *is not* arising only from late-time processes, but from a combination of early- and late-time universe physics. Following this procedure we use the $\Omega_m h$ measurement from the m-only analysis of BOSS LRGs data for $0.2 \leq z \leq 0.75$ (red contours of Fig. 2, $\Omega_m h = 0.220^{+0.029}_{-0.019}$, without the BBN prior on ω_b), with the Ω_m constraint from the uncalibrated BAO of the full BOSS+eBOSS sample: $\Omega_m = 0.299 \pm 0.016$, see table 4 of [15], which includes clustering measurements of low-redshift galaxies, LRGs, Emission Line Galaxies, quasars and Lyman-α emission lines (or $\Omega_m = 0.330 \pm 0.037$ without Lyman-α). The $\Omega_m h$ and Ω_m measurements are considered uncorrelated as they come from different physical effects and different scales (m is almost uncorrelated with standard BAO variables, left panel in Fig. 1). We find $H_0 = 73.6^{+10.5}_{-7.5}$, (or $H_0 = 66.7^{+12.1}_{-10.1}$ without Lyman-α, where the change is solely driven by the determination of $\Omega_{\rm m}$), independent of any prior on ω_b, or the absolute length of the BAO standard ruler. We also report the value of H_0 obtained from applying *ShapeFit* to the LRG sample in combination of a BBN prior on ω_b (this is what is shown in the right panel of Fig. 1): $H_0 = 66.0^{+2.0}_{-1.7}$.

To quantify the impact of the known imaging systematics on cosmological constraints we repeat the above analysis by setting the systematic weights to unity in the BOSS catalogues (i.e., no correction for imaging systematic effects). As shown in Fig. 3 the scaling parameters and $f\sigma_8$ are left largely unchanged while m is affected by a shift of about 2.4 σ. Not unsurprisingly, m "absorbs" systematic effects such as seeing, completeness or extinction angular dependencies: late-time physics constraints from clustering measurements are significantly more robust than early-time physics constraints.

Finally, the advantage offered by a model-independent approach like *ShapeFit* can be appreciated by devising a situation where the internal consistency check fails.

It is well known that a primordial non-Gaussianity of the local type induces a scale-dependent bias in the clustering of biased tracers, which is important at very large scales [25, 26]. This scale-dependent bias correction is proportional to the linear bias, the non-Gaussianity parameter $f_{\rm NL}$ and has a scale dependence $\sim 1/k^2$, hence a leakage of this signal into m can be expected. We forecast the performance of *ShapeFit* and FM by generating mock power spectrum monopole and quadrupole signals

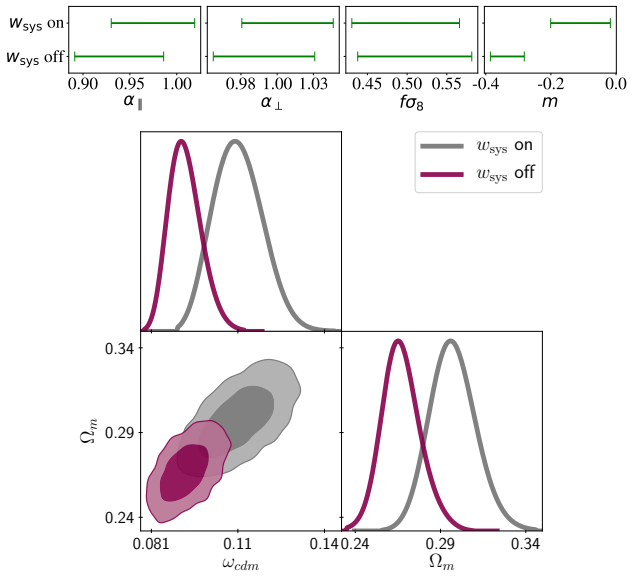


FIG. 3. Effect of turning on and off the imaging systematic weights of BOSS data: for *ShapeFit* in its compressed set of physical variables (upper panels); and for the FM fit in the $\Omega_m - \omega_{cdm}$ plane (lower panel). For *ShapeFit* $f\sigma_8$ and $\alpha_{\parallel,\perp}$ are barely affected by this correction, whereas m absorbs most of the effect; for FM fit, ω_{cdm} and Ω_m are significantly biased.

according to 2-loop resummed perturbation theory, and analyzing it as done for the BOSS NGC $0.5 \leq z \leq 0.75$ data with the same covariance matrix. For choices of bias parameters consistent with the bias of BOSS galaxies ($b \sim 2.2$), the effective redshift of BOSS and including only $k > 0.01h$ Mpc^{-1}, we find that a $f_{\rm NL} = \pm 60$ induces a change in m of $\Delta m = \mp 0.08$ or, in general (linear response validated also for intermediate values), $\Delta m = -0.0013 f_{\rm NL}$, leaving all other physical parameters unaffected. This is shown in the left panel of Fig. 4: the presence of non-zero $f_{\rm NL}$ does not bias the recovery and cosmological interpretation of $\alpha_\parallel$, $\alpha_\perp$ and $f\sigma_8$.

The right panel of Fig. 4 shows the effect on $\omega_{\rm cdm}$ and $\Omega_{\rm m}$ (other cosmological parameters are unaffected) of applying the FM pipeline to the same datasets containing a primordial non-Gaussian signal. Since the FM analysis avoids the compression step, the bias induced by $f_{\rm NL}$ directly propagates into model parameters, without the possibility to diagnose where the signal actually comes from, as it is the case in the *ShapeFit* approach. This indicates that in the presence of non-zero $f_{\rm NL}$, a FM analysis assuming Gaussian initial conditions would recover biased results for Ω_m and ω_{cdm}. The difference in χ^2-estimation between the fit for $f_{\rm NL} = 0$ and that for $f_{\rm NL} = 60$ is $\Delta\chi^2 = 5$ for FM (54 data points, 10 parameters), indicating that a "goodness-of-fit" test relying on χ^2 values would not be enough to signal any issue.

It is important to note that the scale-dependent bias effect of $f_{\rm NL}$ is usually considered negligible at scales $k > 0.03h$ Mpc^{-1}, hence the leakage of $f_{\rm NL}$ on m for *ShapeFit* and the shift in ω_{cdm} and Ω_m for FM, is expected to

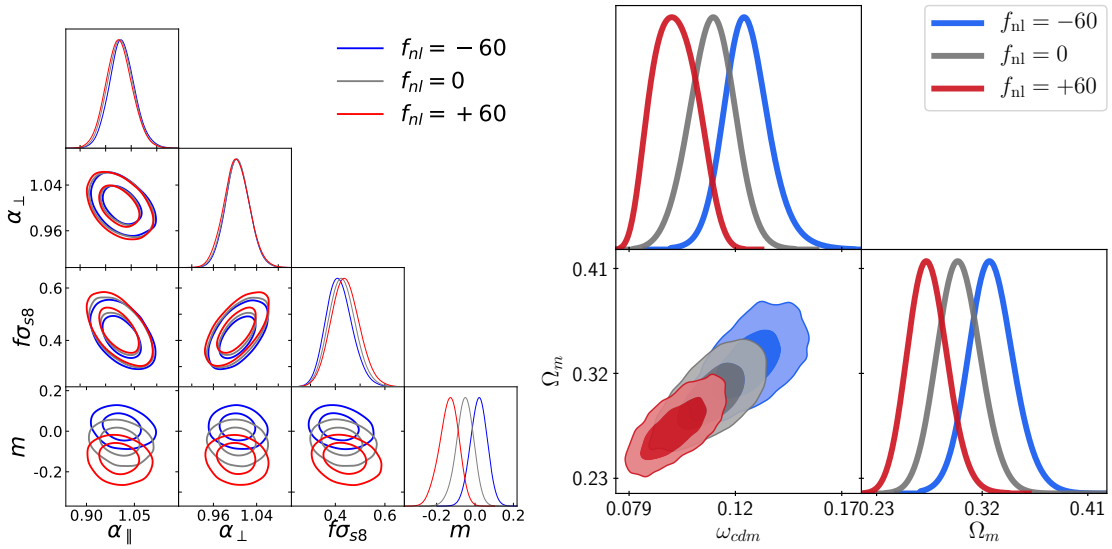


FIG. 4. Systematic bias caused by ignoring in the modelling a $f_{\rm NL}$-signal which is present in the data-vector. In this case we have imprinted a mock $f_{\rm NL} = \pm 60$ signal, which is represented by red and blue contours. For *ShapeFit* (left panel) this systematic effect only impacts the shape parameter m leaving $f\sigma_8$ and the scaling parameters unaffected. For the the FM fit (right panel) it biases both Ω_m and ω_{cdm}.

become significantly more important for surveys volumes that probe scales $k < 0.01h$ Mpc^{-1} not included here.

IV. CONCLUSIONS

For the BOSS dataset the shape-parameter efficiently captures the extra information that FM approaches deliver. *ShapeFit*, by working in terms the compressed variables, has essentially three main advantages over FM.

Model-independence and computing time. Once constraints on the physical variables are obtained they can be interpreted within multiple cosmological models at minimum computational cost. On the other hand, the full modelling approach requires to re-run the full analysis for each new choice of cosmology.

Physical Insight. The physical variables are naturally directly related to specific physical processes that happen in the Universe at different epochs. The scaling factors and the growth of perturbations are sensitive only to the late-time physics of the Universe. The shape parameter captures the shape of the power spectrum on large-scales ($\sim$ to the horizon size at $z \gtrsim 1000$) which contains signatures of early-time physics. For a given cosmological model the early- and late-time effects are intrinsically related, which *i)* sets an internal model-prior implicit in the full model approach but made explicit in the *ShapeFit*; *ii)* the early- and late-time physical variables can be used to perform a powerful consistency test of the cosmological model.

Systematics control. The *ShapeFit* analysis (as well as classic) naturally separates the cosmological information into variables which have very different systematic budgets. The BAO-inferred signal has been shown to be extremely robust to theoretical and observing systematics, with a conservative error budget for state-of-the art measurements of $\lesssim 1\%$ [27]. The amplitude of velocity fluctuation can suffer from imaging and spectroscopic systematics if these are not exquisitely taken into account. The current estimate for this systematic budget is $\simeq 2\%$ [28]. The shape parameter can severely suffer from observational large-scale systematics (e.g., extinction, seeing, completeness). For BOSS data we quantify that the known imaging systematic produces a $\sim 2.4\sigma$ shift in m if not corrected. On the other hand, it absorbs non-standard early-universe physics signals and prevents them to leak into and bias the determination of late-time parameters shaping the expansion/growth history.

We envision that the connection between the physical variables proposed by *ShapeFit* and the full modeling approach will provide a transparent bridge between model-independent and model-dependent interpretation of forthcoming galaxy redshift surveys and a direct physical understanding of their clustering results.

Acknowledgements. H.G-M. and S.B. acknowledge the support from la Caixa Foundation (ID100010434) with code LCF/BQ/PI18/11630024. L.V. acknowledges support of European Unions Horizon 2020 research and innovation programme ERC (BePreSySe, grant agreement 725327). Funding for this work was partially provided by the Spanish MINECO under projects PGC2018-098866-B-I00 FEDER-EU. Funding for SDSS-III has been provided by the Alfred P. Sloan Foundation, the Participating Institutions, the National Science Foundation, and the U.S. Department of Energy Office of Science. The SDSS-III web site is http://www.sdss3.org/.

[1] C. Alcock and B. Paczynski, An evolution free test for non-zero cosmological constant, Nature **281**, 358 (1979).

[2] N. Kaiser, Clustering in real space and in redshift space, Mon. Not. Roy. Astron. Soc. **227**, 1 (1987).

[3] W. J. Percival and M. White, Testing cosmological structure formation using redshift-space distortions, Mon. Not. Roy. Astron. Soc. **393**, 297 (2009), arXiv:0808.0003 [astro-ph].

[4] A. Kosowsky, M. Milosavljevic, and R. Jimenez, Efficient cosmological parameter estimation from microwave background anisotropies, Phys. Rev. **D66**, 063007 (2002), arXiv:astro-ph/0206014 [astro-ph].

[5] Y. Wang and P. Mukherjee, Robust dark energy constraints from supernovae, galaxy clustering, and three-year wilkinson microwave anisotropy probe observations, Astrophys. J. **650**, 1 (2006), arXiv:astro-ph/0604051.

[6] Z. Zhai, C.-G. Park, Y. Wang, and B. Ratra, CMB distance priors revisited: effects of dark energy dynamics, spatial curvature, primordial power spectrum, and neutrino parameters, JCAP **07**, 009, arXiv:1912.04921 [astro-ph.CO].

[7] B. Audren, J. Lesgourgues, K. Benabed, and S. Prunet, Conservative Constraints on Early Cosmology: an illustration of the Monte Python cosmological parameter inference code, JCAP **1302**, 001, arXiv:1210.7183 [astro-ph.CO].

[8] L. Verde, J. L. Bernal, A. F. Heavens, and R. Jimenez, The length of the low-redshift standard ruler, Mon. Not. Roy. Astron. Soc. **467**, 731 (2017), arXiv:1607.05297 [astro-ph.CO].

[9] M. M. Ivanov, M. Simonovi, and M. Zaldarriaga, Cosmological Parameters from the BOSS Galaxy Power Spectrum, JCAP **2005**, 042, arXiv:1909.05277 [astro-ph.CO].

[10] G. D'Amico, J. Gleyzes, N. Kokron, K. Markovic, L. Senatore, P. Zhang, F. Beutler, and H. Gil-Marn, The Cosmological Analysis of the SDSS/BOSS data from the Effective Field Theory of Large-Scale Structure, JCAP **2005**, 005, arXiv:1909.05271 [astro-ph.CO].

[11] S. Alam *et al.* (BOSS), The clustering of galaxies in the completed SDSS-III Baryon Oscillation Spectroscopic Survey: cosmological analysis of the DR12 galaxy sample, Mon. Not. Roy. Astron. Soc. **470**, 2617 (2017), arXiv:1607.03155 [astro-ph.CO].

[12] L. Verde, T. Treu, and A. G. Riess, Tensions between the Early and the Late Universe, in *Nature Astronomy 2019*, Vol. 3 (2019) p. 891, arXiv:1907.10625 [astro-ph.CO].

[13] E. Di Valentino, A. Melchiorri, and J. Silk, Planck evidence for a closed Universe and a possible crisis for cosmology, Nat. Astron. **4**, 196 (2019), arXiv:1911.02087 [astro-ph.CO].

[14] S. Brieden, H. Gil-Marn, and L. Verde, ShapeFit: Extracting the power spectrum shape information in galaxy surveys beyond BAO and RSD, Journal of Cosmology and Astro-Particle Physics **0**, 000 (2021), arXiv:2106.07641 [astro-ph.CO].

[15] S. Alam *et al.* (eBOSS), Completed SDSS-IV extended Baryon Oscillation Spectroscopic Survey: Cosmological implications from two decades of spectroscopic surveys at the Apache Point Observatory, Phys. Rev. **D103**, 083533 (2021), arXiv:2007.08991 [astro-ph.CO].

[16] J. L. Bernal, T. L. Smith, K. K. Boddy, and M. Kamionkowski, Robustness of baryon acoustic oscillation constraints for early-Universe modifications of Λ CDM cosmology, Phys. Rev. D **102**, 123515 (2020), arXiv:2004.07263 [astro-ph.CO].

[17] T. Brinckmann and J. Lesgourgues, MontePython 3: boosted MCMC sampler and other features, Phys. Dark Univ. **24**, 100260 (2019), arXiv:1804.07261 [astro-ph.CO].

[18] D. Blas, J. Lesgourgues, and T. Tram, The Cosmic Linear Anisotropy Solving System (CLASS). Part II: Approximation schemes, Journal of Cosmology and Astro-Particle Physics **2011**, 034 (2011), arXiv:1104.2933 [astro-ph.CO].

[19] A. Chudaykin, M. M. Ivanov, O. H. E. Philcox, and M. Simonović, Nonlinear perturbation theory extension of the Boltzmann code CLASS, Phys. Rev. D **102**, 063533 (2020), arXiv:2004.10607 [astro-ph.CO].

[20] Other than homogeneity, isotropy, and scale-independent growth. The reconstruction step assumes that gravity at mildly non-linear scales is well described by GR.

[21] E. G. Adelberger *et al.*, Solar fusion cross sections II: the pp chain and CNO cycles, Rev. Mod. Phys. **83**, 195 (2011), arXiv:1004.2318 [nucl-ex].

[22] O. Pisanti, A. Cirillo, S. Esposito, F. Iocco, G. Mangano, G. Miele, and P. D. Serpico, PArthENoPE: Public Algorithm Evaluating the Nucleosynthesis of Primordial Elements, Comput. Phys. Commun. **178**, 956 (2008), arXiv:0705.0290 [astro-ph].

[23] N. Schneberg, J. Lesgourgues, and D. C. Hooper, The BAO+BBN take on the Hubble tension, JCAP **1910**, 029, arXiv:1907.11594 [astro-ph.CO].

[24] J. L. Bernal, L. Verde, and A. G. Riess, The trouble with H0, Journal of Cosmology and Astro-Particle Physics **10**, 019 (2016).

[25] N. Dalal, O. Dore, D. Huterer, and A. Shirokov, The imprints of primordial non-gaussianities on large-scale structure: scale dependent bias and abundance of virialized objects, Phys. Rev. **D77**, 123514 (2008), arXiv:0710.4560 [astro-ph].

[26] S. Matarrese and L. Verde, The effect of primordial non-Gaussianity on halo bias, Astrophys. J. Lett. **677**, L77 (2008), arXiv:0801.4826 [astro-ph].

[27] G. Merz *et al.*, The clustering of the SDSS-IV extended Baryon Oscillation Spectroscopic Survey quasar sample: Testing observational systematics on the Baryon Acoustic Oscillation measurement, Mon. Not. Roy. Astron. Soc. **0**, 000 (2021), arXiv:2105.10463 [astro-ph.CO].

[28] A. Smith *et al.*, The Completed SDSS-IV Extended Baryon Oscillation Spectroscopic Survey: N-body Mock Challenge for the Quasar Sample, Mon. Not. Roy. Astron. Soc. **499**, 269 (2020), arXiv:2007.09003 [astro-ph.CO].